Chapter 4

The Fabry Perot Resonator

4.1 General Aspects

Whether a steady state radiation field can be established in an optical resonator depends on the wavelength of the radiation and on the mirror spacing. Steady state means that both the amplitude and the phase reproduce themselves after one round trip. It is easy to understand that both conditions can only be accomplished if the resonator length is an integral multiple of half the wavelength. Only in this case can we obtain standing waves inside the resonator with nodal intensity points on the mirror surfaces (Fig. 4.1). The preceding statement is always true as long as the field is not confined laterally by means of apertures. Hence, for a given mirror spacing L_0 and a medium with index of refraction n between the mirrors, we will find steady state field distributions for all wavelengths λ_q for which the following condition holds:

$$\lambda_q = \frac{2\,L}{q} \tag{4.1}$$

with:

λ_q	:	wavelength in vacuum
$L=L_0 n$	:	optical path length between mirrors
L_0	:	geometrical path length between mirrors
n	:	index of refraction

The integral number q, called the axial mode order, represents the number of intensity maxima. A resonator thus exhibits a periodic sequence of resonance frequencies $\nu_q=c_0/\lambda_q$ which are separated by:

$$\Delta\nu = \frac{c_0}{\lambda_q} - \frac{c_0}{\lambda_{q+1}} = \frac{c_0}{2\,L} \tag{4.2}$$

with c_0 being the speed of light in vacuum. For an optical path length of $L=1m$ - a typical length for laser resonators - the frequency gap is 150 MHz, which is extremely small compared to the frequency of visible light ($\nu=6\text{x}10^8$ MHz for λ=500nm). The axial mode order q, which represents the number of half wavelengths fitting between the mirrors, is very high: for λ=500nm, we will find $4\text{x}10^6$ intensity maxima.

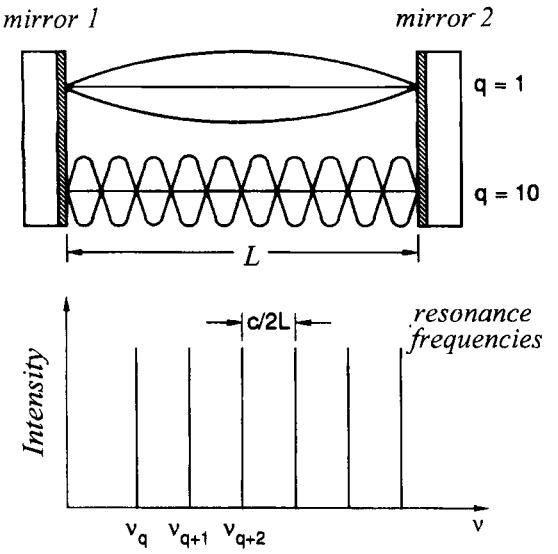

Fig. 4.1 Steady state field distributions in an optical resonator can only be established if the distance between the mirrors is an integral multiple q of half the wavelength. Due to the interference between the two fields moving in opposite directions, a standing wave pattern is created. The corresponding resonance frequencies are separated by a gap of $c/2L$, where c is the speed of light inside the resonator.

Standing waves of the kind shown in Fig. 4.1 can only be found if the resonator does not experience losses due to output coupling. If the combined mirror reflectivity R_1R_2 is less than 100%, traveling wave components will be generated too. The intensity minima will then not be equal to zero anymore. The resonance condition (4.1), which determines the wavelengths generating the maximum intracavity power density, is also valid for lossy resonators, but the resonance peaks depicted in Fig. 4.1 will become broader as the loss in the resonator is increased. That means that even wavelengths that do not exactly match the resonance condition (4.1) will induce a resonant behavior inside the resonator.

In the following we shall discuss the basic resonance properties of optical resonators without taking the transverse field structure into account. This is a reasonable approach since the transverse mode structure will only induce variations to the resonance conditions rather than changing the overall physical behavior of the resonator. As will be presented in Part III, the transverse field distribution splits each axial resonance frequency ν_q into a set of frequencies, each corresponding to a transverse mode structure.

We will start with the most basic optical resonator, the plane-parallel Fabry Perot interferometer (FPI), which has many applications in laser engineering and optical measurement techniques. The influence of the mirror reflectivities on the resonance frequencies and on the bandwidth will be presented. The incorporation of an active medium into the FPI will automatically lead to the basic properties of lasers. In Sec 4.3 we will apply the knowledge about FPIs to optical coatings whose characteristics can be investigated by treating them as a series of FPIs. The goal of this section is to make the reader familiar with the physical properties of resonator mirror coatings. A knowledge of coating designs and techniques is essential to understand the impact of the coating on the resonator design and on the beam characteristics of a laser.

4.2 The Fabry Perot Interferometer

4.2.1 Passive Fabry Perot Interferometer

A Fabry Perot interferometer (FPI) consists of two mirrors with reflectivities R_1, R_2, respectively, and are separated by a distance L (Fig. 4.2). For convenience, we assume that both mirrors are planar and are not confined by an aperture. The diffraction of the light can then be neglected and beam propagation inside the FPI can be described by means of geometrical optics. Losses generated by scattering and absorption on the mirror surfaces are incorporated into our resonator model by placing a medium with loss factor V between the mirrors. The loss factor represents the fraction of incident light intensity that is transmitted by the medium [2.14, 2.15].

Monochromatic light at a wavelength λ entering the FPI with an intensity I_0 (electric field E_0) will be partially reflected by mirror 1. The transmitted intensity portion is then reflected back and forth between the two mirrors. With each reflection intensity is coupled out of the FPI in both the forward and the backward direction. Summation of all waves coupled out yields the transmission T and the reflectance R of the FPI. If r_1, r_2 denote the reflection coefficients and t_1,t_2 are the corresponding transmission coefficients of the two mirrors, the reflected field E_r and the transmitted field E_t are given by (with V being the amplitude loss factor):

$$E_r = E_0 \left[r_1 - t_1^2 v^2 r_2 \exp[i2kL] \sum_{n=0}^{\infty} (v^2 r_1 r_2 \exp[i2kL])^n \right] \tag{4.3}$$

$$E_t = - E_0 \, t_1 t_2 v \, \exp[ikL] \sum_{n=0}^{\infty} (v^2 r_1 r_2 \exp[i2kL])^n \tag{4.4}$$

Note that a transmission phase factor of $\exp(i\pi/2)$ has to be taken into account to get the minus signs [2.1].

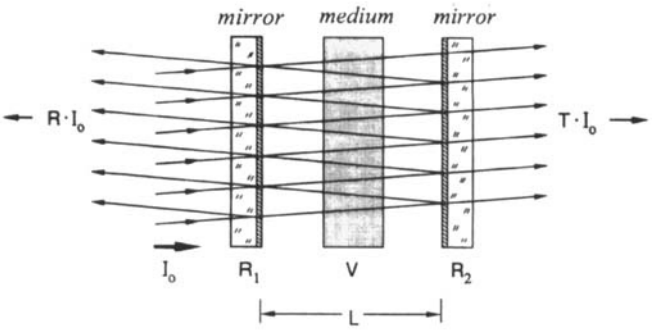

Fig. 4.2 Plane-parallel Fabry Perot interferometer (FPI). Incoming light with intensity I_0 is oscillating between the two mirrors and is partially transmitted with each reflection at a mirror. The rays are shown tilted to show the propagation in a more convenient way.

By calculating the intensities from (4.3) and (4.4), we can determine the fraction of the incident intensity I_0 being transmitted and reflected by the FPI:

$$R = \frac{(\sqrt{R_1}-\sqrt{R_2}V)^2 + 4\sqrt{R_1R_2}V\sin^2(kL)}{(1-\sqrt{R_1R_2}V)^2 + 4\sqrt{R_1R_2}V\sin^2(kL)} \tag{4.5}$$

$$T = \frac{(1-R_1)(1-R_2)V}{(1-\sqrt{R_1R_2}V)^2 + 4\sqrt{R_1R_2}V\sin^2(kL)} \tag{4.6}$$

with:

R_i = $|r_i|^2$: reflectivity of mirror i
V = $|v|^2$: loss factor per transit
k = $2\pi/\lambda$: wave number
λ : wavelength in vacuum
L : optical mirror spacing

Transmission T and reflectance R as a function of the phase kL are shown in Fig. 4.3 for a loss free FPI with $R_1=R_2$. The transmission becomes maximum if the condition

$$\sin(kL) = 0 \quad \Rightarrow \quad \lambda = \frac{2L}{q} \quad , q=1,2,3,... \tag{4.7}$$

holds. The transmission T thus exhibits a periodic sequence of maxima whose frequencies are separated by $c_0/2L$, called the *free spectral range*. As discussed in Sec. 4.1, standing waves are generated inside the FPI at these resonance frequencies characterized by the condition that the mirror spacing equals an integral multiple of half the wavelength. The following relations hold:

Maximum Transmission:

$$T_{max} = \frac{(1-R_1)(1-R_2)V}{(1-\sqrt{R_1R_2}V)^2} \tag{4.8}$$

$$T_{max} = 1 \qquad \text{for } R_1=R_2,\ V=1$$

Maximum Energy Density:

$$\rho_{max} = \frac{I_0}{c_0}\frac{1-R_1^2}{(1-\sqrt{R_1R_2}V)^2} \tag{4.9}$$

$$\rho_{max} = I_0(1+R)/[c_0(1-R)] \qquad \text{for } R_1=R_2,\ V=1$$

Bandwidth (FWHM):

$$\delta\nu = |\ln(\sqrt{R_1R_2}V)|\frac{c_0}{2\pi L} \tag{4.10}$$

Free Spectral Range:

$$\Delta\nu = \frac{c_0}{2L} \tag{4.11}$$

Light will be transmitted by the FPI if its frequency lies within the frequency width $\delta\nu$ of one of the resonance peaks. The resonance frequencies, determined by a maximum of the transmission T, exhibit a frequency width that decreases as the mirror reflectivities and the loss factor are increased. The reflectance R of the FPI is minimum at the resonance frequencies, since the waves traveling out of the FPI in the backwards direction partially cancel due to destructive interference. If both mirror reflectivities are equal, complete destructive interference occurs and consequently the reflectance of the FPI goes to zero at the resonance frequencies (if $V=1$). For the loss free FPI, the relation $R+T=1$ always holds.

It seems surprising that the transmission of a loss free FPI at a resonance frequency is equal to one, which means that the incident beam intensity is completely transmitted even though both mirrors exhibit reflectances of higher than zero. Even for mirror reflectances of $R_1=R_2=0.9999$, no intensity is reflected off the FPI. This puzzling phenomenon is caused by the interference of all waves bouncing back and forth inside the FPI and being transmitted through the two mirrors. In resonance, the waves inside the FPI exhibit constructive interference leading to an increase of the intracavity intensity I such that the intensity transmitted through mirror 2 equals the initial beam intensity I_0 . For $R_1=R_2=0.9999$ the intracavity intensity is 10,000 times higher than the intensity I_0 of the beam incident on the FPI. Figure 4.4 depicts the resonant behavior of the intracavity intensity I as a function of kL.

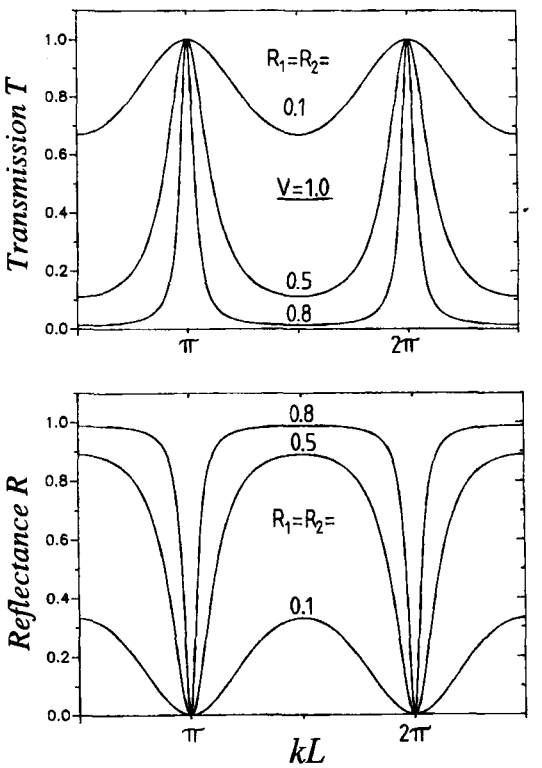

Fig. 4.3 Transmission and reflectance of a loss free FPI ($V=1$) as a function of kL. Transmission maxima are observed when the optical mirror spacing L equals an integral multiple of half the vacuum wavelength. Energy conservation requires $R+T=1$.

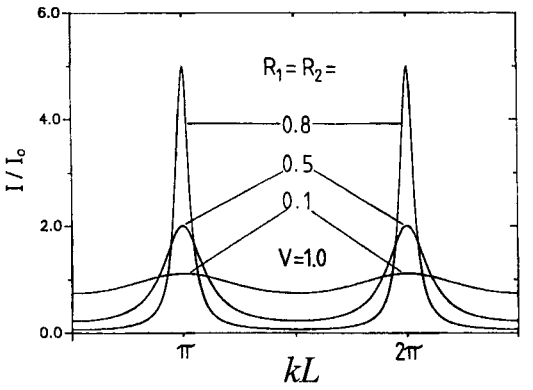

Fig. 4.4 Intensity I inside the FPI (normalized to the incident intensity I_0) as a function of kL for a loss free symmetric FPI ($V=1$).

If the light source is shut off, the energy stored inside the FPI will show a temporal decay due to the output coupling losses experienced on both mirrors. The decay time τ after which the fraction of 1/e (≈ 0.368) of the initial energy has remained inside the FPI is given by:

$$\tau = \frac{L}{c_0} \frac{1}{|\ln(\sqrt{R_1 R_2} V)|} = \frac{1}{2\pi\delta\nu} \tag{4.12}$$

The decay time also determines the time it takes the FPI to be fully operational after the light source is switched on again. As in all linear resonant systems, the decay time and the resonance bandwidth are inversely proportional.

Two quantities, the finesse F and the cavity quality Q, are commonly used to characterize the quality of a FPI. They are defined as:

$$F = \frac{\Delta\nu}{\delta\nu} = \frac{\textit{free spectral range}}{\textit{bandwidth}} = \frac{\pi}{|\ln(\sqrt{R_1 R_2} V)|} \tag{4.13}$$

$$Q = 2\pi\Delta\nu\tau = \frac{\nu}{\delta\nu} \tag{4.14}$$

High quality FPIs exhibit both a high finesse and a high cavity quality. This is accomplished by choosing the mirror reflectivities R_1, R_2 and the loss factor V as close to 1.0 as possible. Table 4.1 compares the resonance properties of a typical FPI used in atomic physics for the measurement of spectral lines with those of a spring oscillator. FPIs used for the active stabilization of laser frequencies have finesses of up to 30,000.

Table 4.1 Resonance properties of an FPI and a spring oscillator.

	FPI	spring oscillator
Resonance frequency	$\nu=4.94\times10^{14}$ Hz (λ=607nm)	2 Hz
Axial mode number	q=33,000	-
Bandwidth	$\delta\nu=3.8\times10^{8}$ Hz	0.1Hz
Free spectral range	$\Delta\nu=1.5\times10^{10}$ Hz	-
Max. transmission	T=0.13	-
Decay time	$\tau=3.61\times10^{-10}$ s	1.6 s
Cavity quality	$Q=1.3\times10^{6}$	20
Finesse	F=39.5	-

If the loss factor of the FPI is less than one which means that the light bouncing back and forth inside the FPI experiences losses due to absorption or scattering, the transmission T of the FPI cannot reach its maximum value of $T_{max}=1.0$ at the resonant frequencies. We can calculate the loss ΔV^* of the FPI by inserting Eqs. (4.5) and (4.6) into the condition for energy conservation:

$$R + T + \Delta V^* = 1$$

This results in:

$$\Delta V^* = (1-V)\frac{(1-R_1)(1+R_2V)}{(1-\sqrt{R_1R_2}V)^2 + 4\sqrt{R_1R_2}V\sin^2(kL)} \tag{4.15}$$

where $1-V$ is the loss per transit inside the FPI. Before we visualize this equation in a graph, we should try to understand what to expect. As already seen in Fig. 4.4, the intracavity intensity is amplified at the resonance frequencies to values which, for FPIs with high cavity quality Q (high mirror reflectivities), can exceed the initial beam intensity by several orders of magnitude . A higher intracavity intensity will, however, generate a higher loss ΔV^* of the FPI. If, for instance, the intracavity intensity is 20 times higher than the initial intensity I_0, a loss of 1% per transit will generate a loss in intensity of 20% in terms of the initial intensity. The loss of the FPI will therefore show maxima at the resonance frequencies and the maximum loss will increase as the mirror reflectivities are increased. One can also use the decay time,τ, to discuss the loss of an FPI. At the resonance frequencies the light remains inside the FPI for a long time. The increased number of reflections induce a high loss since for each transit the amount $(1-V)$ of the intensity is absorbed or scattered. A long decay time (which is equivalent to having high mirror reflectances R_1,R_2 or a small bandwidth $\delta\nu$), therefore, generates a high loss ΔV^* of the FPI. It is for this reason that FPIs with a high transmission T_{max} and a small bandwidth are difficult to realize.

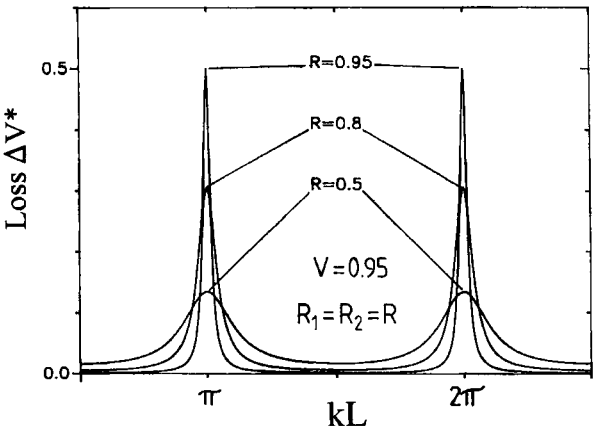

Fig. 4.5 Loss of an FPI with mirror reflectances $R_1=R_2=R$ as a function of kL. The loss per transit is 5% ($V=0.95$).

Figure 4.5 shows the loss of a symmetric FPI as a function of kL for a loss per transit of 5%. As discussed, the maximum loss occurs at the resonance frequencies. Note that the loss of the FPI is usually higher than the loss per transit. For high mirror reflectivities, in particular, the loss can exceed 50% even though the loss per transit may be only 1%. This interesting result indicates how sensitive the properties of an optical resonators are to small losses induced inside the resonator. In Chapter 10 we will present models for the calculation of the output power of laser resonators. We will see that small losses in the few percent range induced by scattering or absorption in the active medium (or on the mirror surfaces) can decrease the output power by up to one order of magnitude, depending on the gain of medium. With the above discussion of the FPI this is not surprising: the high number of bounces inside the resonator magnifies the loss.

It is worth noting that the FPI can be designed such that its reflectance R vanishes at the resonance frequencies even if losses occur between the mirrors. By using (4.5), the condition to meet is found to be:

$$R_1 = R_2 V^2$$

A FPI for which this relation holds is called *impedance-matched*. This is not the case for the FPIs in Fig. 4.6 in which the maximum loss ΔV^*_{max} and the maximum transmission T_{max} are plotted as a function of the mirror reflectances $R=R_1=R_2$. This is why in this figure the loss of the FPI vanishes as the mirror reflectivities approach unity: the incoming beam is 100% reflected by the FPI.

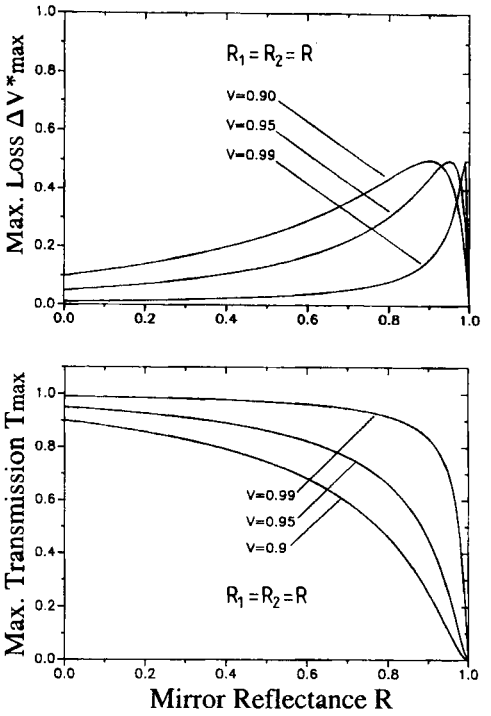

Fig. 4.6 Maximum loss and maximum transmission of an FPI at the resonance frequencies as a function of the mirror reflectances $R=R_1=R_2$. In each graph the three curves correspond to a loss of 1%, 5%, and 10% per transit. Even with small losses inside the FPI, high transmission with a small bandwidth (equivalent to high mirror reflectivities) is difficult to attain.

4.2.2 Applications of FPIs

Since the transmission of an FPI is a function of both the optical mirror spacing L and the wavelength λ of the incident light, the FPI can be used to measure small variations in lengths, or to determine the spectral characteristics of a light source, Furthermore, it can serve as a filter to decrease the spectral width of the light source [2.7-2.9, 2.11]. An example demonstrating the length measurement capabilities of an FPI, Fig. 4.7 depicts an experimental set-up to measure the expansion characteristics of a piezo ceramic. The piezo ceramic is driven by an AC voltage which results in an oscillating movement of one mirror of the FPI. The FPI used here has concave mirrors, preferably with the center of curvature located on the opposite mirror (confocal FPI) This geometry provides the lowest sensitivity to mirror tilt [2.13]. The transmitted intensity of a laser beam with known wavelength λ is measured with a photodiode as a function of the drive voltage. A sequence of transmission maxima is observed corresponding to a piezo movement of $\lambda/2$ from maxima to maxima. By using these data, the variation in piezo length as a function of the applied voltage can be determined. With such a set-up it is possible to resolve length differences on the order of nanometers (10^{-9}m).

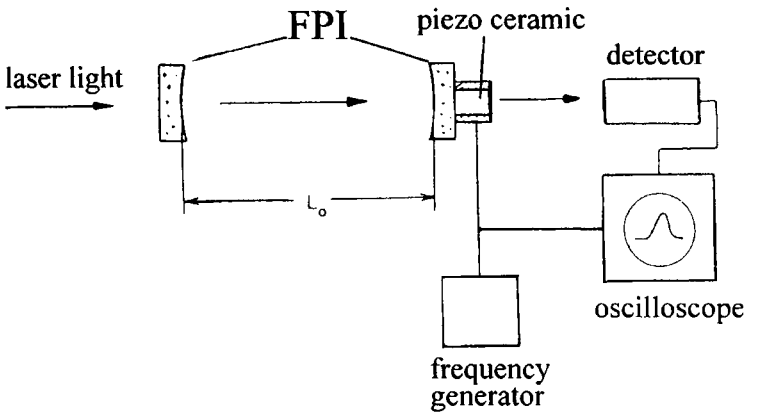

Fig. 4.7 Experimental set-up for measuring the expansion characteristic of a piezo ceramic [2.9].

This arrangement can also be used to measure the spectral characteristics of a laser beam. However, the bandwidth of the laser must be smaller than the free spectral range of the FPI, otherwise we will get maximum transmission for several wavelengths simultaneously. Furthermore, the bandwidth of the FPI should be as small as possible to get high frequency resolution. It is for these reasons that FPIs with small mirror spacings (10 mm) and high mirror reflectivities are used for laser frequency measurements. Typical free spectral ranges are on the order of 10 GHz with bandwidths around 10 MHz (for spectral properties of lasers see Table 4.2). The laser with known wavelength λ is used as a calibration standard to relate each drive voltage of the piezo to a certain wavelength. After replacing the laser with the unknown laser, the spectral distribution of the latter can be observed on the oscilloscope. The spectrum of a HeNe laser shown in Fig. 4.11 was recorded using this technique.

The spectral filtering properties of the FPI are used in **etalons**, which are fixed spaced FPIs with cavity lengths varying from 10 mm down to 0.1 mm. They are either made of two coated plano-plano glass plates (air gap etalon) or they consist of one plate coated on both sides. The latter technique provides higher transmission and higher damage threshold. Etalons exhibit free spectral ranges of up to 1,000 GHz with a Finesse of 50. The resonance wavelengths λ_q can also be changed to a certain degree by tilting the etalon. If θ denotes the tilt angle, the new resonance wavelengths are given by $\lambda'_q = \lambda_q / \cos\theta$.

Higher free spectral ranges are realized with **interference filters**. They can be considered as a stack of several FPIs with mirror spacings on the order of μm. Technically, these filters are generated by coating multilayer dielectric films on top of each other with dielectric spacers in between representing the mirror gap. Bandwidths are on the order of 10^4 GHz (this corresponds to about 10nm for visible wavelengths) and free spectral ranges of 10^5 GHz (100nm) are obtained. In addition, higher order transmission peaks can be suppressed by adding colored filter glass. At the desired wavelength, the typical transmission of interference filters is 50%.

4.2.3 Fabry Perot Interferometer with Gain - Laser Resonator

We now consider the case that the medium placed inside the FPI amplifies the light oscillating between the two mirrors. The gain factor G with $G>1$ denotes the factor by which the intensity has been amplified after a transit through the medium. In the passive FPI discussed in the last section, the intensity I incident on the medium was decreased to VI after the transit. With light amplification taken into account, the intensity at the other side of the medium is given by GVI. We can therefore use all equations derived in Sec. 4.2 and take the gain into account by replacing V with GV. Equations (4.8)-(4.11) then yield:

Resonance frequencies: $$\nu_q = q\frac{c_0}{2L} \qquad q = 1,2,3, \ldots$$

Free spectral range: $$\Delta\nu = \frac{c_0}{2L}$$

Bandwidth: $$\delta\nu = |\ln(G\sqrt{R_1R_2}V)|\frac{c_0}{2\pi L} \approx \frac{\Delta\nu}{\pi}(1-G\sqrt{R_1R_2}V)$$

Decay time: $$\tau = \frac{L}{c_0}\frac{1}{|\ln(G\sqrt{R_1R_2}V)|} \approx \frac{L}{c_0}\frac{1}{1-G\sqrt{R_1R_2}V}$$

Maximum transmission: $$T_{max} = \frac{(1-R_1)(1-R_2)GV}{(1-G\sqrt{R_1R_2}V)^2}$$

The resonance frequencies are not affected by the gain of the medium. A more detailed theory shows that the resonance frequencies are shifted by the gain, but the shift is negligible for most applications (see Sec. 9.6). The bandwidth of the active FPI is decreased as the gain of the active medium is increased. This is understandable because the losses that the light experiences per round trip are now partially compensated by the active medium. This results in an increase of both the decay time and the transmission of the FPI. The insertion of an active medium is a well established technique to enhance the spectral resolution of an FPI. However, the gain of the medium should not overcompensate the losses generated by output coupling at the mirrors, absorption, and scattering. In other words, the total gain loss product should not exceed 1.0:

$$G\sqrt{R_1R_2}V < 1$$

If the gain factor G is chosen so that all losses are exactly compensated:

$$G\sqrt{R_1R_2}V = 1 \tag{4.16}$$

our mathematical model predicts that the decay time, the transmission, and the energy density inside the FPI diverge. The wave summation used to derive (4.3) and (4.4) is not applicable in this case, especially since the gain factor G is affected by the increasing intensity inside the FPI. When the threshold condition $GRV=1$ holds, the spontaneous emission of the active medium leads to the generation of standing light waves inside the FPI, even without an external light source. The FPI has now become a laser resonator [2.6].

A laser resonator thus emits light at the resonance frequencies ν_q if (4.16) holds for the gain factor G at these frequencies. The corresponding electromagnetic waves - these are standing waves if both mirror reflectivities are equal - are referred to as the axial modes of the resonator. They are characterized by the mode number q, which determines the number of half wavelengths fitting into the optical resonator length.

The gain factor G depends on the frequency and the intensity of the light inside the resonator and it can be increased by transferring more power into the active medium via the pump process (e.g. flashlamp pumping or laser diode pumping for solid state lasers, gas discharge for gas lasers). Without the pumping process, the gain is less than 1.0, which means that the light is absorbed as it propagates through the medium. In general, the gain factor G can exceed 1.0 only at distinct frequencies which are characteristic for the active material used. By using special mirror coating designs, the laser emission is usually restricted to one of these possible emission wavelengths (the mirror reflectivities are chosen too low at the other wavelengths to reach the threshold condition (4.16)). Figure 4.8 shows the gain profile at the preferred laser emission wavelength of ruby for four different pump powers. A threshold pump power is required to reach a gain factor G of more than 1.0.

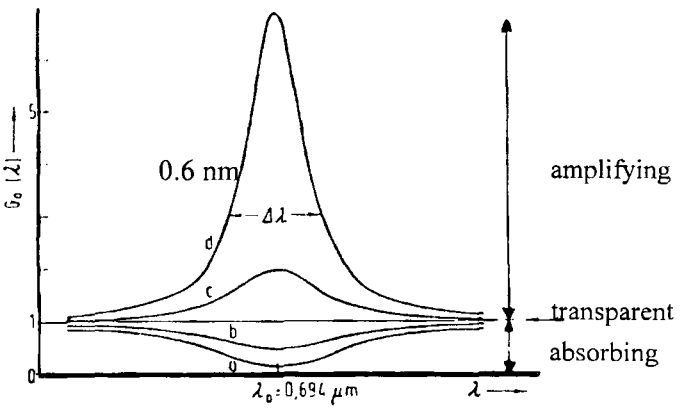

Fig. 4.8 Laser materials exhibit gain profiles only at characteristic wavelengths. This example shows gain profiles for a ruby crystal at $\lambda=694nm$ for four different pump powers (a-d). The axial modes whose wavelengths are within the bandwidth can oscillate in the laser resonator.

Laser emission can only be generated within the bandwidth of the gain profile. The number of axial modes, to a good approximation, is given by the ratio of the gain bandwidth to the free spectral range of the resonator. The bandwidth of the laser emission strongly varies with the active material used. Some gas lasers have gain bandwidths as low as 100 MHz, whereas dye lasers can exceed this value by more than a factor of 10,000. Accordingly, the number of axial modes varies considerably with the type of laser. Table 4.2 gives an overview of the spectral emission characteristics of common lasers including the number of axial modes that may oscillate in a resonator with an optical length of 1m. In homogeneously broadened lasers, the number of observed axial modes is much smaller. Alexandrite and Ti:sapphire lasers, for instance, exhibit laser bandwidths of less than 10nm.

Table 4.2 Center wavelength λ_0, gain bandwidth $\Delta\lambda$, and number of axial modes n within the gain bandwidth (resonator with optical length 1m) for different lasers.

Medium	Type of Laser	λ_0[nm]	$\Delta\lambda$[nm]	n
KrF	excimer	249	20	646,000
Ar^+	gas	488	0.003	3
HeNe	gas	632.8	0.002	10
CO_2	gas	10,600	2	36
Rhodamin 6G	dye	600	60	334,000
GaAlAs	semiconductor	804	2	6,200
Alexandrite	solid state	760	70	240,000
Nd:glass	solid state	1,054	10	18,000
Nd:YAG	solid state	1,064	0.5	885
Nd:YLF	solid state	1,047	1.0	1,825
Yb:YAG	solid state	1,030	20	38,000
Ti:sapphire	solid state	800	200	635,000

What happens if the gain is so high that GRV is greater than 1.0? The consequence would be that the intensity inside the resonator is increased more by the gain than it is decreased by the losses. The intensity would therefore become infinite! This catastrophic behavior is prevented by the saturation of the gain. The gain factor is decreased as the intensity of the light is increased. The intensity dependence of the gain factor is given by (see Sec. 9.5):

$$G = \exp\left[\frac{g_0 l}{(1 + I/I_S)^x}\right] \tag{4.17}$$

The *small-signal gain* $g_0 l$ is proportional to the inversion, which for four-level lasers increases linearly with the pump power. The saturation intensity I_S is a characteristic of the laser material. The quantity x depends on the type of medium used. The two limits are $x=1$ for homogeneously broadened media and $x=0.5$ for inhomogeneously broadened media (see Sec. 9.5 on line broadening). How does the gain saturation influence the oscillation of axial modes in a laser ? Let us assume that we cover one resonator mirror to prevent laser oscillation and we pump the active medium. Since we have negligible intensity inside the resonator (the losses are too high to start laser oscillation) the gain factor (4.17) is given by:

$$G_0 = \exp(g_0 l) \tag{4.18}$$

The small-signal gain factor G_0 determines how light with an intensity much smaller than the saturation intensity gets amplified by the medium in one transit. As soon as we remove the cover on the resonator mirror, all axial modes for which the relation $G_0 RV \geq 1$ holds will oscillate. The intensity of the modes will now rapidly increase. According to (4.17), the gain factor will decrease resulting in a continuous decrease of the net amplification of the light. Finally, a steady state intensity is reached for which $GRV=1$ holds. By using (4.17), we find the steady state intensity to be:

$$I = I_S \frac{(g_0 l)^{1/x} - |\ln(RV)|^{1/x}}{|\ln(RV)|^{1/x}} \tag{4.19}$$

When the laser is inhomogeneously broadened all axial modes which started to oscillate will reach this steady state intensity (as shown in Fig. 4.9). For truly homogeneously broadened lasers, only one axial mode will oscillate in steady state, since competition between modes occurs (we shall discuss this phenomenon in detail in Sec. 9.5). Note that it is the gain saturation that makes a laser work! The intensity dependence of the gain ensures that we get a steady state solution for the intensity and thus a well defined output power from the laser.

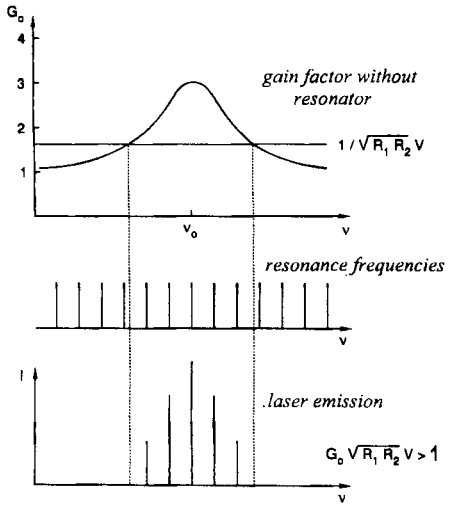

Fig. 4.9 Only axial resonator modes for which $G_0 RV > 1$ holds can oscillate. Due to saturation, the gain factor will decrease as the mode intensity increases. In steady state the intensity in each axial mode is determined by $GRV=1$, with G given by (4.17).

Figure 4.9 presents the spectral emission characteristics of a laser resonator. Only the axial modes of the resonators for which the small signal gain factor G_0 is high enough to overcome the losses generated by absorption and output coupling will oscillate. The steady state intensity is highest for the modes that experienced the highest small signal gain. For an inhomogeneously broadened active medium, oscillation of all these axial modes is observed because each mode depletes the gain only at its resonance frequency without interacting with other modes. The envelope of the axial mode intensity spectrum is then determined by the gain profile of the medium (Figs. 4.10 and 4.11). For homogeneously broadened lasers, however, only the highest gain mode survives due to the fact that all axial modes have access to the whole gain profile (see Sec. 9.5). This holds as long as no thermal or mechanical distortions occur and spatial hole-burning is prevented.

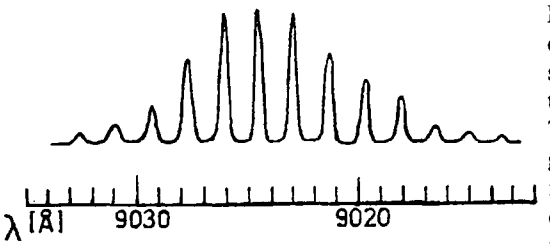

Fig. 4.10 Axial mode intensity spectrum of a GaAs diode laser (measured with a scanning FPI). The polished endfaces of the crystal serve as the resonator mirrors. The short resonator length (L_0=*1mm*) generates a large free spectral range. This is the reason why only 13 axial modes are observed even though the gain bandwidth is quite large.

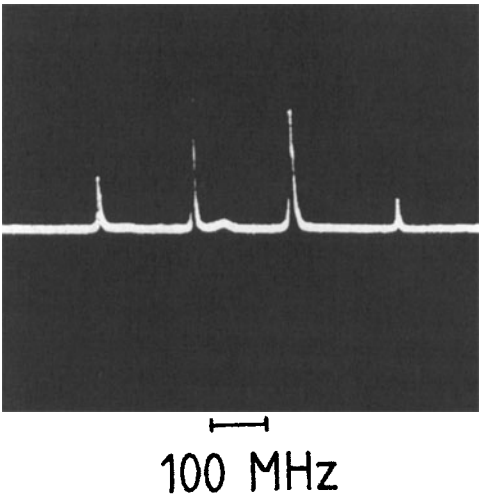

Fig. 4.11 Spectrum of a HeNe laser (λ_0=*632.8nm*) measured with a scanning FPI. The optical resonator length is L=*0.7m*. The small gain bandwidth allows only four axial modes to oscillate.

With increasing pump power the gain profile increases resulting in a wider frequency range within which the gain is high enough to overcome the resonator losses. For an inhomogeneously broadened laser, new axial modes will be added at the outer areas of the gain profile. The mode numbers n shown in Table 4.2 represent upper limits achievable at high pump powers. In a laser, the bandwidth $\delta\nu$ of each axial mode can assume very low values. According to the theory of the active FPI, the bandwidth of a laser in steady state oscillation should be zero. In reality, however, the bandwidth is much larger due to spontaneous emission which generates a noise background to the axial mode build up by induced emission. The noise determines the lower bandwidth limit theoretically attainable in a laser (see the Schawlow-Townes formula in Sec. 9.7). Furthermore, the resonator set-up experiences small scale optical length variations due to vibrations and temperature changes. The effect of the length variations on the bandwidth is generally several orders of magnitude higher compared to the influence of the noise.

By using special stabilizing and feedback techniques, bandwidths as low as 100 mHz can be realized. Without active or passive frequency stabilization, laser modes exhibit bandwidths on the order of MHz. In general, many axial modes are found in the spectral emission of a laser resonator (see Table 4.2) since true homogeneously broadened lasers which operate at one axial mode are not very common. Without additional frequency selecting elements inside the resonator, the bandwidth of inhomogeneously broadened lasers is determined by the bandwidth of the gain profile. The technical realization of narrow bandwidths or single axial mode operation in these lasers requires the incorporation of etalons into the resonator. In homogeneously broadened lasers, oscillation at one axial mode can be forced by using resonator designs that prevent spatial hole burning. A detailed discussion of single mode lasers shall be given in Chapter 21.

4.3 Optical Coatings

4.3.1 A Coating Design Matrix Method

The principle of the FPI can be used to generate optical elements that exhibit spectral reflectances suitable for a desired application. We have seen that an FPI has its highest reflectance R if the mirror spacing is an odd multiple of quarter wavelengths. A preferred technique to realize such an FPI is to coat a substrate with a dielectric material whose optical thickness nL equals one quarter wavelength (Fig. 4.12a). The two mirror reflectances R_1 and R_2 are now given by the reflectances of the two dielectric interfaces, air-coating and coating-substrate. Unfortunately, this design provides only limited control over the amplitude and the spectral profile of the reflectance R. In order to become more flexible in the design of the reflection properties, multi-layer coatings of different dielectric materials are used as depicted in Fig. 4.12b. This is the preferred way to produce resonator mirrors and anti-reflection coatings of optical elements [2.4,2.5,2.16,2.17]. In the following we will derive a matrix method to calculate the reflectance of such a stack of layers deposited onto a substrate [2.1].

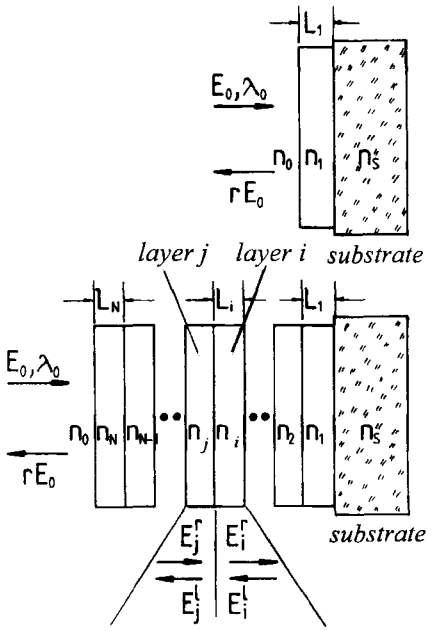

Fig. 4.12 a) An FPI can be realized by coating a substrate with dielectric material. If the thickness L_1 is an odd multiple of $\lambda_0/(4n)$, the reflectance becomes a maximum at the wavelength λ_0. b) A multi-layer coating enhances the flexibility in designing spectral reflectance profiles r(λ).

In order to keep the discussion as general as possible we assume that the thickness of each layer can be chosen arbitrarily. We will, however, restrict ourselves to normal incidence. Incorporation of a tilt of the surface normal with respect to the wave propagation vector can be accomplished by modifying the final result.

Let a beam with field amplitude E_0 and wavelength λ_0 be incident on the stack of layers as shown in Fig. 4.12b. Reflection and transmission at each interface inside the stack leads to the generation of two counterpropagating waves in each layer. Our goal is to calculate the amplitude of the wave leaving the stack in the direction opposite to the incident wave. We first consider one interface in the stack between layer i and layer j and determine how the electric field amplitudes propagating in opposite directions are related to one another. If r_{ij}, r_{ji} denote the reflection coefficients for a transition from layer i to layer j and from layer j to layer i, respectively, and t_{ij},t_{ji} are the corresponding transmission coefficients, we obtain:

$$E_j^l = t_{ij}E_i^l + r_{ji}E_j^r \tag{4.20}$$

$$E_i^r = r_{ij}E_i^l + t_{ji}E_j^r \tag{4.21}$$

Since we want to express the fields in layer j as a function of the fields in layer i we rewrite (4.21) as:

$$E_j^r = \frac{1}{t_{ji}} E_i^r - \frac{r_{ij}}{t_{ji}} E_i^l \tag{4.22}$$

The second equation is obtained by inserting (4.22) into (4.20):

$$E_j^l = \frac{r_{ji}}{t_{ji}} E_i^r + \frac{t_{ij}t_{ji} - r_{ji}r_{ij}}{t_{ji}} E_i^l \tag{4.23}$$

By using the Fresnel relations $t_{ij}=t_{ji}$ (the transmission cannot depend on the propagation direction) and $r_{ij}=-r_{ji}$ (a phase shift of π is induced when the light is reflected off the high index material) together with $r_{ij}^2+t_{ij}^2=1$ (energy conservation), we can write Eqs. (4.22) and (4.23) in the form of a matrix equation:

$$\begin{pmatrix} E_j^l \\ E_i^r \end{pmatrix} = \frac{1}{t_{ij}} \begin{pmatrix} 1 & -r_{ij} \\ -r_{ij} & 1 \end{pmatrix} \begin{pmatrix} E_i^l \\ E_i^r \end{pmatrix} = T_{ij} \begin{pmatrix} E_i^l \\ E_i^r \end{pmatrix} \tag{4.24}$$

Hence, we found the transition matrix T_{ij} connecting the field amplitudes on both sides of the interface between layer i and layer j. Now we have to incorporate the propagation of the fields inside each layer from right to left. We take layer j and mark the field after propagation with an asterisk. The propagation will induce a phase shift on both field components as well as an amplitude loss factor V (note that for the field propagating to the right we have to subtract the phase and divide by the loss factor to get the amplitude on the left side of the layer!). The propagation matrix P_j can be written as:

$$\begin{pmatrix} E_j^{*l} \\ E_j^{*r} \end{pmatrix} = \begin{pmatrix} v_j \exp[i\frac{2\pi}{\lambda_0} n_j L_j] & 0 \\ 0 & \frac{1}{v_j} \exp[-i\frac{2\pi}{\lambda_0} n_j L_j] \end{pmatrix} \begin{pmatrix} E_j^l \\ E_j^r \end{pmatrix} = P_j \begin{pmatrix} E_j^l \\ E_j^r \end{pmatrix} \tag{4.25}$$

In the substrate we have only one field amplitude E_S propagating to the right since there is no reflecting interface to generate a left-propagating wave. Starting at the substrate, we combine all transition matrices T and propagation matrices P until we reach the first interface on the left side of the stack:

$$\begin{pmatrix} rE_0 \\ E_0 \end{pmatrix} = T_{NA} P_N T_{(N-1)N} P_{N-1} \cdots T_{23} P_2 T_{12} P_1 T_{S1} \begin{pmatrix} 0 \\ E_S \end{pmatrix} \tag{4.26}$$

where T_{NA} and T_{SI} are the transition matrices from layer N to the outer medium and from the substrate to the first layer, respectively. The whole multi-layer stack can thus be described by the stack matrix S with:

$$\begin{pmatrix} rE_0 \\ E_0 \end{pmatrix} = \begin{pmatrix} S_{11} & S_{12} \\ S_{21} & S_{22} \end{pmatrix} \begin{pmatrix} 0 \\ E_S \end{pmatrix} = S \begin{pmatrix} 0 \\ E_S \end{pmatrix} \tag{4.27}$$

The reflection coefficient r of the stack can now be calculated to be:

$$r = \frac{S_{12}}{S_{22}} \tag{4.28}$$

In general, the reflection coefficient r is a complex number which means that the field experiences a phase shift. The reflectance R and the phase shift ϕ read:

$$R = rr* = \left|\frac{S_{12}}{S_{22}}\right|^2 \tag{4.29}$$

$$\phi = atan\left[\frac{Im(r)}{Re(r)}\right] \tag{4.30}$$

Note that this matrix method of calculating the reflectance is equivalent to the wave summation method used for the FPI! All the field components in (4.24) represent the sums of the partial waves which means that the interference is taken into account.

To verify the equivalency of the two methods let us try to derive the reflectance R of an FPI. We use only one layer of thickness L and refractive index n with reflection coefficients r_1 and r_2 at the front and the rear interface, respectively. The stack matrix S then reads:

$$S = T_1 P_1 T_2 = \frac{1}{t_1 t_2} \begin{pmatrix} 1 & -r_1 \\ -r_1 & 1 \end{pmatrix} \begin{pmatrix} v \exp[i\frac{2\pi}{\lambda_0} Ln] & 0 \\ 0 & \frac{1}{v} \exp[-i\frac{2\pi}{\lambda_0} Ln] \end{pmatrix} \begin{pmatrix} 1 & -r_2 \\ -r_2 & 1 \end{pmatrix}$$

Equation (4.29) yields for the reflectance of the FPI:

$$R = \left| \frac{r_1 - r_2 v^2 \exp[i4\pi nL/\lambda_0]}{1 - r_1 r_2 v^2 \exp[i4\pi nL/\lambda_0]} \right|^2 \tag{4.31}$$

This is equivalent to the square of the reflection coefficient determined by the wave sum (4.3), with $k=2\pi n/\lambda_0$.

The calculation of the reflectance R for multilayer coatings using the stack matrix method can become quite a task if it is done manually. It is much more convenient (especially because one gets the same result when the calculation is repeated!) to use a computer to perform the algebra. Input parameters of such a coating design program are the layer thicknesses, their indices of refraction and the angle of incidence of the light. The reflection coefficients r_{ij} are given by the Fresnel equations [1.1,1.2]. For a transition from layer i to layer j with normal incidence, the reflection coefficient does not depend on the polarization of the incident beam. The Fresnel equations yield:

$$r_{ij} = \frac{n_i - n_j}{n_i + n_j} \tag{4.32}$$

Note that r_{ij} is negative if the beam is reflected off the higher index material. If the normal of the substrate is tilted by an angle θ_A with respect to the wave vector of the incident beam (Fig. 4.13), we first have to calculate the angle of refraction θ_j for each layer j by using Snell's law. If n_A denotes the index of refraction of the outside medium (usually this is air), the angles θ_j are determined by:

$$\cos\theta_j = \sqrt{1 - \frac{n_A^2}{n_j^2}\sin^2\theta_A} \tag{4.33}$$

The propagation matrix $\boldsymbol{P}_j$ for each layer then has the form:

$$\boldsymbol{P}_j = \begin{pmatrix} v_j \exp[i\frac{2\pi}{\lambda_0} n_j L_j \cos\theta_j] & 0 \\ 0 & \frac{1}{v_j} \exp[-i\frac{2\pi}{\lambda_0} n_j L_j \cos\theta_j] \end{pmatrix} \tag{4.34}$$

The reflection coefficients r_{ij}, to be inserted into the transition matrix $\boldsymbol{T}_{ij}$, are different for s-polarized and p-polarized light.

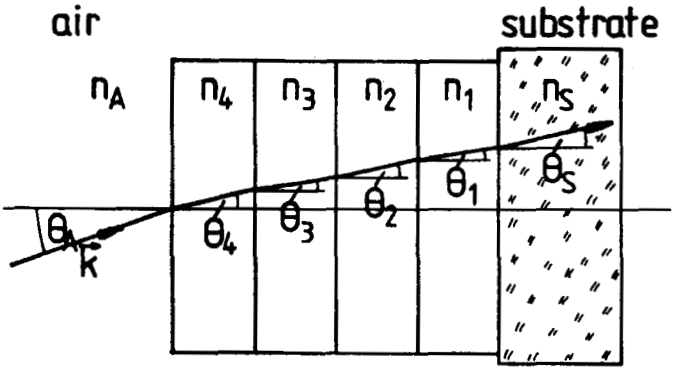

Fig. 4.13 Angles of refraction in each layer for incidence at an angle θ_A.

The coefficients are given by the Fresnel equations:

$$s\text{-}polarized: \quad r_{ij} = \frac{n_i\cos\theta_i - n_j\cos\theta_j}{n_i\cos\theta_i + n_j\cos\theta_j} \tag{4.35}$$

$$p\text{-}polarized: \quad r_{ij} = \frac{n_j\cos\theta_i - n_i\cos\theta_j}{n_j\cos\theta_i + n_i\cos\theta_j} \tag{4.36}$$

The stack matrices for the two polarizations have to be calculated separately. Tilted multilayer coatings generally exhibit different reflectances R for the two polarizations.

4.3.2 Quarter Wavelength Systems

Single λ/4 Layer

We consider one dielectric layer with index of refraction n_1 and geometrical thickness L_1. The index of refraction of the substrate and the outer medium are n_S and n_A, respectively. According to (4.32), the reflection coefficients are given by:

$$r_{S1} = \frac{n_S - n_1}{n_S + n_1}, \qquad r_{1A} = \frac{n_1 - n_A}{n_1 + n_A}$$

Application of (4.29) to the stack matrix results in the reflectance:

$$R = \frac{n_1^2(n_s-n_A)^2\cos^2\delta + (n_1^2-n_S n_A)^2\sin^2\delta}{n_1^2(n_s+n_A)^2\cos^2\delta + (n_1^2+n_S n_A)^2\sin^2\delta} \tag{4.37}$$

with: $$\delta = \frac{2\pi}{\lambda_0} n_1 L_1$$

If we choose an optical thickness of a quarter wavelength for the design wavelength λ_0 ($L_1=\lambda_0/(4n_1)$), the reflectance assumes its maximum of:

$$R_{max} = \left[\frac{n_1^2 - n_A n_S}{n_1^2 + n_A n_S}\right]^2 \tag{4.38}$$

For such a $\lambda/4$ layer, the reflectance as a function of the wavelength varies between this maximum value (at the wavelengths $\lambda_0/(2q+1)$) and the reflectance of the bare substrate (at the wavelengths $\lambda_0/(2q)$) given by:

$$R_{min} = \left[\frac{n_S - n_A}{n_S + n_A}\right]^2 \tag{4.39}$$

For the latter wavelengths, the layer represents a $\lambda/2$ coating which does not affect the reflectance of the substrate. Due to dispersion (the refractive indices increase as the wavelength is decreased), the reflectance maxima are shifted towards longer wavelengths. Figure 4.14 shows the transmission spectrum for a single layer of Ta_2O_5 with a geometrical thickness of 1050nm ($n_1=2.1$), coated on a BK7 glass substrate ($n_S=1.5$). The outside medium is air ($n_A=1.0$). This coating represents a quarter wavelength layer for λ_0=8,820nm. If there were no dispersion, we would also expect the maximum reflectance of $R_{max}=0.242$ at the wavelengths ($q=2$-5): 1,764nm, 1,260nm, 980nm, and 802nm. Considering the fact that the transmission curve includes the reflectance of the rear substrate interface as well as absorption losses in the substrate, the measured maximum reflectance is in good agreement with (4.38). Note the spectral shifts of the transmission minima at shorter wavelengths due to dispersion. Measured dispersion curves for different coating materials and coating conditions are presented in Fig. 4.15.

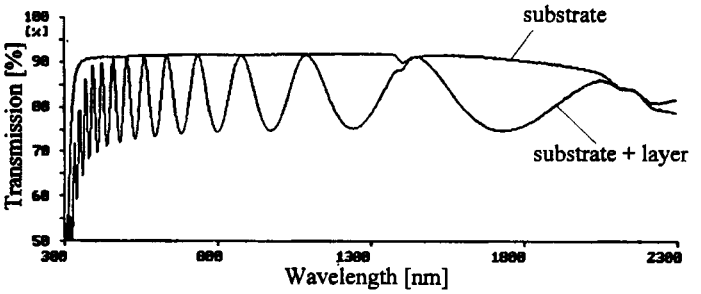

Fig. 4.14 Transmission spectrum for a single layer of Ta_2O_5 (n=*2.1*) on a BK7 substrate (n_S=*1.5*). The geometrical layer thickness is *1,050nm*. The transmission spectrum of the plain substrate is also shown for comparison. The layer was deposited using ion beam sputtering with argon [S.1].

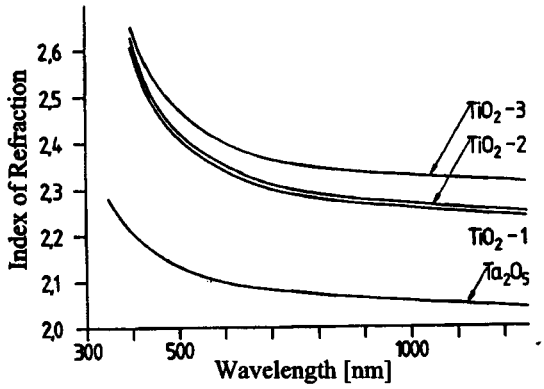

Fig. 4.15 Measured index of refraction of single layers of TiO_2 and Ta_2O_5 with an optical thickness of 2,120nm at a wavelength of λ_0=1,060nm (deposited with ion beam sputtering). Equation (4.37) was used to determine the refractive index from the spectral transmission minima. The three TiO_2 layers were coated using different source materials and different O_2 atmospheres [S.1].

As can be seen from (4.38), the reflectance of the substrate is increased by the quarter wavelength coating if the index of refraction n_1 of the layer is greater than the index of refraction n_S of the substrate. If we choose a lower index material for the coating, the reflectance of the substrate can be decreased. In order to completely suppress the substrate reflectance (antireflection coating), the index of refraction n_1 must be chosen such that the following condition holds:

$$n_1 = \sqrt{n_A n_S} \tag{4.40}$$

For a glass substrate (n_S=*1.5*) in air, we thus need an index of refraction of n_1=*1.225*. The coating material exhibiting an index close to this value is magnesium fluoride (n_1=*1.37 at 600nm*). A MgF_2 coating lowers the reflectance of a glass/air interface from 4% to about 1%.

Multiple λ/4 Layers

Let k be the number of λ/4 layers with geometrical thickness:

$$L_j = \frac{\lambda_0}{4n_j(\lambda_0)}$$

deposited onto the substrate. Note that in the notation we use, the layer with refractive index n_1 and thickness L_1 is always the one in contact with the substrate. The reflectance R at the wavelength λ_0 is given by:

$$R = \left[\frac{(n_1n_3n_5...n_{k-1})^2n_A - n_S(n_2n_4...n_k)^2}{(n_1n_3n_5...n_{k-1})^2n_A + n_S(n_2n_4...n_k)^2}\right]^2 \qquad \textit{for } k \textit{ even}\ ,\ k\geq 2 \qquad (4.41)$$

$$R = \left[\frac{(n_1n_3n_5...n_k)^2 - n_Sn_A(n_2n_4...n_{k-1})^2}{(n_1n_3n_5...n_k)^2 + n_Sn_A(n_2n_4...n_{k-1})^2}\right]^2 \qquad \textit{for } k \textit{ odd}\ ,\ k\geq 3 \qquad (4.42)$$

Usually, alternating layers of two coating materials - a high index material (n_H=*1.9-4.2*) and a low index material (n_L=*1.35-1.46*) with $n_L<n_S<n_H$ - are evaporated onto the substrate. The above equations can then be simplified:

$$R = \left[\frac{n_1^k n_A - n_S n_2^k}{n_1^k n_A + n_S n_2^k}\right]^2 \qquad \textit{for } k \textit{ even}\ ,\ k\geq 2 \qquad (4.43)$$

$$R = \left[\frac{n_1^{k+1} - n_S n_A n_2^{k-1}}{n_1^{k+1} + n_S n_A n_2^{k-1}}\right]^2 \qquad \textit{for } k \textit{ odd}\ ,\ k\geq 3 \qquad (4.44)$$

For a multilayer antireflection coating, the first layer deposited onto the substrate has to be the high index material (with refractive index $n_1=n_H$). From (4.43) and (4.44) we get the conditions for zero reflectance:

$$\left(\frac{n_1}{n_2}\right)^k = \frac{n_S}{n_A}\ ,\quad k \textit{ even} \qquad (4.45)$$

$$\left(\frac{n_1}{n_2}\right)^{k+1} = \frac{n_An_S}{n_2^2}\ ,\quad k \textit{ odd} \qquad (4.46)$$

These conditions are much easier to meet than the single layer condition (4.40). If a large number of multiple quarter wavelength layers are used, the reflectance of the substrate will be enhanced and will eventually reach 100%. In order to attain the desired reflectance with a minimum number of layers, it is advantageous to choose coating materials which exhibit a large difference in their index of refraction. Resonator mirrors for lasers emitting in the visible and near infrared spectral range are usually produced by applying up to 15 alternating dielectric layers on glass or quartz substrates. Figure 4.16 shows how the reflectance of the substrate at the design wavelength λ_0 varies with an increasing number of layers for different dielectric materials. Spectrally resolved reflectance curves for case c) of this figure are presented in Fig. 4.17 for a center wavelength $\lambda_0 = 460nm$.

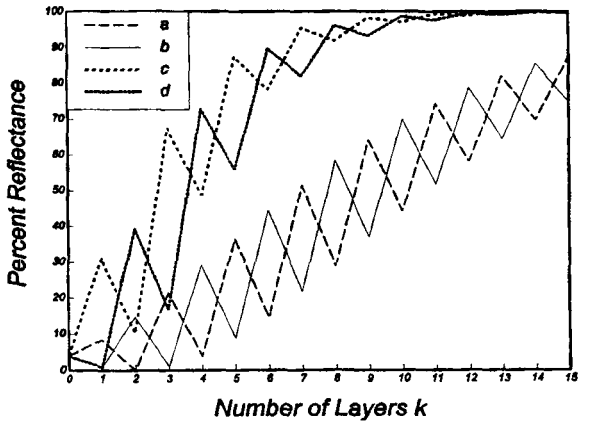

Fig. 4.16 Reflectivity of multilayer quarter wavelength coatings as a function of the number of layers, calculated with (4.43) and (4.44). Alternating coating materials are deposited on a glass substrate ($n_S=1.5$): a) $n_1=1.65$, $n_2=1.35$; b) $n_1=1.35$, $n_2=1.65$; c) $n_1=2.3$, $n_2=1.35$; d) $n_1=1.35$, $n_2=2.3$.

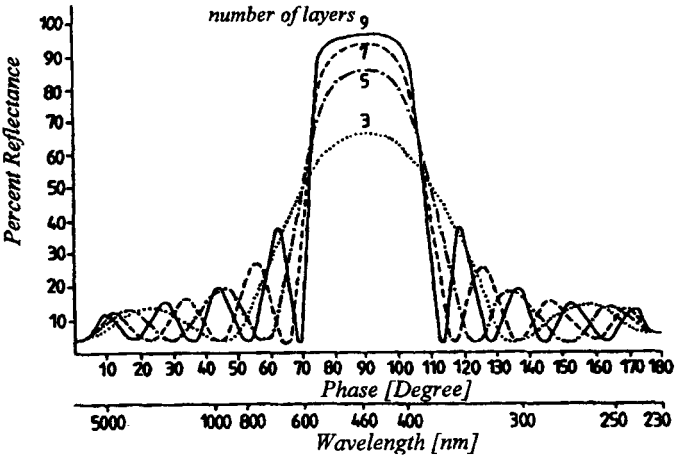

Fig. 4.17 Calculated reflectance as a function of the phase $2\pi Ln/\lambda$ for odd numbers of quarter wave layers with $n_1=2.3$, $n_2=1.35$, and $n_S=1.5$ (high index material deposited first). The lower axis shows the corresponding wavelengths assuming a design wavelength of $\lambda_0=460nm$.

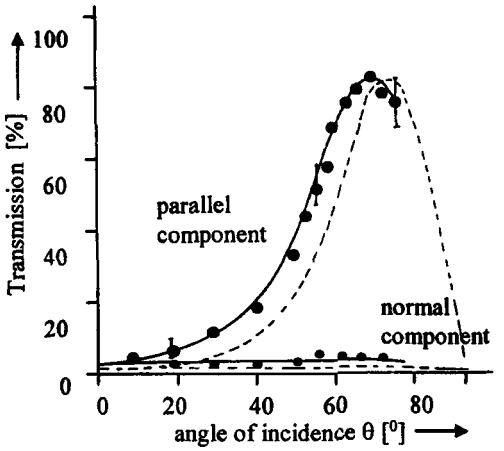

Fig. 4.18 Transmission of a dielectric polarizer vs. the angle of incidence for λ=534nm. Layer structure: five layers of low and five layers of high index material. The broken line represents the calculated transmission.

Dielectric plates can be used to polarize light, as was discussed in Sec. 3.2.1. The degree of polarization increases with the number of stacked plates. The stackplate polarizer can be replaced by a system of thin layers resulting in very efficient and compact polarizers, The calculation of the reflectance of such a thin film polarizer can be done numerically using Eqs. (4.33-4.36). An example is shown in Fig. 4.18.

4.3.3 Coating Methods and Materials

There are different methods to deposit dielectric coatings on a substrate. The most common one is the **evaporation** of the dielectric material onto the substrate in a vacuum chamber at typical pressures of 10^{-6} torr (Fig.4.19). The substrates are mounted on a carousel that rotates on top of the chamber to achieve a homogeneous deposition. The vapor of the coating material is generated at the bottom of the chamber by heating the source material (in the form of a granulate) with an electron beam or, in older machines, by inductance or resistance heating. The thickness of the coating is monitored during the process by analyzing the spectral reflectance of a test substrate. Since evaporation is a thermal process, the low kinetic energy (about 50meV) of the atoms is not high enough to generate a homogeneous coating. The coatings exhibit a certain porosity which leads to a lower refractive index compared to the bulk material and also to a decreased damage threshold. By heating the substrate to temperatures of about 300°C the atoms get additional energy to move on the substrate and thus distribute themselves more evenly. Electron-beam evaporation generates optical coatings with the highest damage threshold to laser radiation. High quality, high reflectivity mirrors can withstand fluences of over 4J/cm^2 at 355nm and over 25J/cm^2 at 1064nm (for 10ns long laser pulses). In cw-operation at 1064nm, high reflectors can withstand power densities of more than 5MW/cm^2.

A higher homogeneity of the coatings can be attained by providing additional energy to the coating atoms. In **ion assisted deposition** techniques, the substrate is bombarded during the deposition with an ion beam transferring additional energy on the order of 100eV per ion to the growing coating. A process of similar energy is the **ion beam sputtering**. A beam of inert ions is aimed at the target and the target atoms are kicked out of the material and land on the substrate with a high energy. Both of these energetic processes generate layers with bulk-like indices of refraction, resulting in a better durability of the coating. The damage threshold, however, is lower as compared to e-beam evaporation, due to intrinsic stress generated in the optical layers.

Table 4.3 Physical properties of coating materials used for laser mirrors. The indices of refraction are those obtained in thermal deposition processes (electron beam evaporation). The transparent spectral range is defined by an absorption coefficient of less than 10^3 per cm [2.4].

Material	index of refraction (at λ_0=500nm)	transparent spectral range
Na_3AlF_6	1.35	0.20 - 14μm
MgF_2	1.37	0.22 - 2 μm
SiO_2	1.46	0.20 - 8 μm
HfO_2	1.95	0.22 - 12μm
ZrO_2	2.10	0.34 - 12μm
Ta_2O_5	2.16	0.30 - 10μm
TiO_2	2.25	0.35 - 12μm
ZnS	2.55	0.38 - 25μm

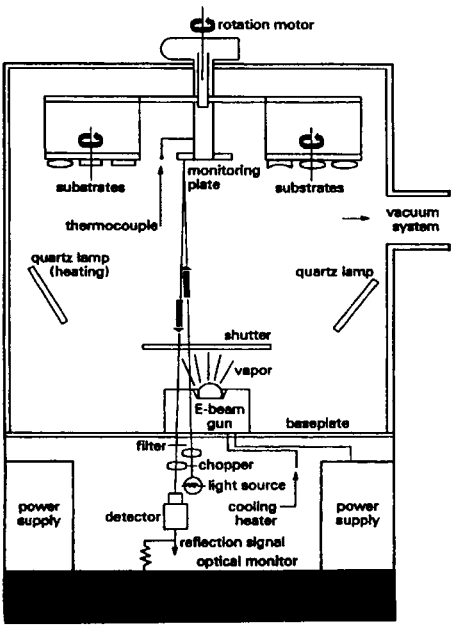

Fig. 4.19 Schematic view of a typical vacuum deposition chamber with electron beam heating [S.2] (courtesy of Melles-Griot, Irvine, CA). The electron beam is aimed at the coating material contained in water-cooled crucibles. The crucibles are located to the side of the electron beam gun (not shown).

Part III

Passive Open Resonators